An Experimental Comparison of CMG Steering Control Laws

Dongwon Jung* and Panagiotis Tsiotras†
Georgia Institute of Technology, Atlanta, GA 30332-0150

Control moment gyros (CMGs) are spacecraft attitude control actuators which act as torque amplifiers. They are thus suitable for attitude hold and reorientation of large spacecraft or for slew maneuvering. They provide the necessary torques via gimballing a spinning flywheel. A major problem encountered with the use of CMGs in practice is the possibility of singularities for certain combinations of gimbal angles. In such singular gimbal angle configurations the CMG cluster cannot generate torques along a certain direction. Several singularity avoidance and escape steering logics have been reported in the literature to solve the CMG singularity problem. In this paper, we experimentally compare three of the most common CMG steering logics using a realistic spacecraft simulator. We compare the relative merits of these steering laws with respect to their singularity avoidance capabilities and their efficiency in generating the commanded control torques. An adaptive feedback stabilizing control law is also used in conjunction with each CMG steering law to account for the gravity disturbance torque.

I. Introduction

Control Moment Gyros (CMGs) are actuators that produce a control torque by changing the angular momentum vector direction with respect to the spacecraft reference frame. The major benefit of utilizing CMGs for spacecraft control is their well-known torque amplification property.[1] The flywheel of a CMG spins at a constant speed, and torquing of the gimbal results in a precessional, gyroscopic torque, which is orthogonal to both the spin and gimbal axes. This torque is much larger than the gimbal axis command torque, hence the term "torque amplification." Despite the advantages of CMGs over, say, reaction wheels stemming from their increased torque production capabilities, the employment of CMGs in practice has been hindered by the possibility of geometric singularities.

A singular state for a CMG is a gimbal angle combination at which no torque is possible along a certain direction. Two types of singular states can be identified. *External* or *saturation singularities* occur when the sum of all CMG angular momenta reaches its maximum. This is owing to the fact that a CMG changes only the direction of the angular momentum vector and hence, there exists a maximal momentum surface. External singularities are those gimbal angle combinations, for which the total CMG cluster momentum has reached this surface, since in this case the CMG cluster cannot generate a torque which is directed outward this surface. In addition, there exist singular states at which the total angular momentum is smaller than the maximum. These are

*Ph.D. candidate, School of Aerospace Engineering, Tel: (404) 894-6299, Email: dongwon_jung@ae.gatech.edu. Student Member AIAA.

†Associate Professor, School of Aerospace Engineering, Tel: (404) 894-9526, Fax: (404) 894-2760. E-mail: p.tsiotras@ae.gatech.edu. Associate Fellow AIAA. Corresponding author.

called *internal singularities*.[1] References 2–4 offer a comprehensive analysis and classification of the CMG singularities. A visualization of the angular momentum surface can be found in Refs. 5, 6 and 7.

During maneuvering, the gimbal angles should be steered away from the singular states in order to be able to generate any commanded torque. Many researchers have studied and proposed a variety of methods to avoid or escape the CMG singularities. The simplest, and probably the most common, method is based on the minimum two-norm, pseudo-inverse solution to the gimbal steering equation.[4,8–10] In these methods, the gimbals are steered away from the singular states using finite gimbal rates. As these methods rely on the pseudo-inverse solution for steering the gimbal angles, they do not explicitly avoid or escape the singularities. Instead they steer the gimbal angles towards the singularities and rapidly transit through them with a finite torque error, whenever needed. This compensation torque should have a short duration and its value should be kept at a minimum. Despite the introduced torque error, the methods based on the pseudo-inverse are relatively simple and can be easily implemented online.

Alternative methods have been reported in the literatures for handling the CMG singularities. They can be broadly categorized as local gradient methods and global avoidance methods. The local gradient methods utilize a null motion,[2,11] which does not affect the output torque for a redundant CMG cluster. The null motion direction is searched locally, along with an objective function containing information about the singularities, and then a null motion is applied to avoid the singularities. Even though these methods produce a torque which is exactly the same as the required torque, nonetheless, there still exist singularities which cannot be avoided using these methods. The global avoidance methods[12,13] incorporate global optimization to anticipate the singularities and steer the gimbal angles so that the CMG system does not encounter them. The off-line calculation needed for these methods makes them of limited use for online steering.

In this article, several CMG singularity avoidance steering laws are compared in a realistic three-axis spacecraft simulator. The steering logics tested are all based on the minimum two-norm, pseudo-inverse solution, and they were chosen because they can be efficiently implemented online without the need of any off-line calculations. The basic form of these methods is known as the Singularity Robust (SR) method. Its variations in terms of the singularity avoidance parameters are briefly presented and compared. Each steering law provides the ability to avoid or escape any singularities with finite gimbal rates. Different choices of the singularity avoidance parameters produce different torque errors in the vicinity of singularities. These errors are compared and commented upon.

Since the gravity torque acting on the spacecraft simulator cannot be completely eliminated by balancing, a dynamic state feedback control law is implemented to cancel this gravity torque and improve the final pointing accuracy. This dynamic state feedback attitude control law is a slight modification over the one proposed by Di Gennaro in Ref. 14 for the case of CMGs. During the maneuver the gimbals are steered in accordance to the desired gimbal rate command, which is calculated by the feedback stabilization controller and implemented via the singularity avoidance steering law. The seamless integration of the feedback control law and the feedforward steering logic is crucial for achieving high pointing accuracy, and it is demonstrated in the experimental results.

II. Equations of Motion

The complete equations of motion for a rigid spacecraft with a cluster of N CMGs have been developed in the literature. Here we use the format of Ref. 15, which is repeated below for convenience

$$\dot{J}\omega + J\dot{\omega} + A_{\mathrm{g}} I_{\mathrm{cg}} \ddot{\gamma} + A_{\mathrm{t}} I_{\mathrm{ws}} [\Omega]^d \dot{\gamma} + [\omega^\times]\Big(J\omega + A_{\mathrm{g}} I_{\mathrm{cg}} \dot{\gamma} + A_{\mathrm{s}} I_{\mathrm{ws}} \Omega\Big) = g_e. \tag{1}$$

In Eq. (1) $\omega = (p, q, r)^{\mathsf{T}} \in \mathbb{R}^3$ is the spacecraft angular velocity vector. The matrix J is the inertia matrix of the whole spacecraft, defined as

$$J \triangleq {}^B I + A_{\mathrm{s}} I_{\mathrm{cs}} A_{\mathrm{s}}^{\mathsf{T}} + A_{\mathrm{t}} I_{\mathrm{ct}} A_{\mathrm{t}}^{\mathsf{T}} + A_{\mathrm{g}} I_{\mathrm{cg}} A_{\mathrm{g}}^{\mathsf{T}}, \tag{2}$$

where ${}^B I$ is the combined matrix of inertia of the spacecraft platform and the point-masses of the CMGs. The matrices $I_{\mathrm{c}\star}$ and $I_{\mathrm{w}\star}$ are diagonal, with elements the values of the inertias of the gimbal plus wheel structure and wheel-only-structure of the CMGs, respectively. The vectors $\gamma = (\gamma_1, \ldots, \gamma_N)^{\mathsf{T}} \in \mathbb{R}^N$ and $\Omega = (\Omega_1, \ldots, \Omega_N)^{\mathsf{T}} \in \mathbb{R}^N$ are the gimbal angles and the wheel speeds of the CMGs with respect to the gimbals, respectively. On each CMG we attach a frame located at the center of the gimbal/wheel combination having unit vectors $\hat{e}_{\mathrm{g}j}, \hat{e}_{\mathrm{s}j}, \hat{e}_{\mathrm{t}j}$, $(j = 1, \ldots, N)$ along the gimbal axis, the wheel spin axis, and the torque producing axis, respectively, so that $\hat{e}_{\mathrm{t}j} = \hat{e}_{\mathrm{g}j} \times \hat{e}_{\mathrm{s}j}$. The matrices $A_\star \in \mathbb{R}^{3\times N}$ collect these unit vectors such that $A_\star \triangleq [e_{\star 1}, \cdots, e_{\star N}]$, with $\star = \mathrm{g}, \mathrm{s}$ or t. All the vectors and matrices in (1) are expressed in a body-fixed frame located at the center of rotation of the spacecraft platform.

For any vector $x = (x_1, x_2, x_3)^{\mathsf{T}} \in \mathbb{R}^3$, the notation $[x^\times]$ denotes the skew-symmetric matrix

$$[x^\times] \triangleq \begin{bmatrix} 0 & -x_3 & x_2 \\ x_3 & 0 & -x_1 \\ -x_2 & x_1 & 0 \end{bmatrix},$$

whereas, for a vector $x \in \mathbb{R}^N$ the notation $[x]^d \in \mathbb{R}^{N\times N}$ denotes the diagonal matrix having as elements the components of the vector x, that is,

$$[x]^d \triangleq \mathrm{diag}(x_1, \cdots, x_N).$$

Note that $A_{\mathrm{s}} = A_{\mathrm{s}}(\gamma)$ and $A_{\mathrm{t}} = A_{\mathrm{t}}(\gamma)$ and thus, both matrices A_{s} and A_{t} are functions of the gimbal angles. Consequently, the inertia matrix $J = J(\gamma)$ is also a function of the gimbal angles γ, whereas the matrix ${}^B I$ is constant. The time variation of the inertia matrix is reflected in the first term of (1). This variation of the inertia matrix due to the changes of the gimbal angles is typically small in practice (at least for small size wheels), and could have been neglected in the following developments without sacrificing much of the rigor. Nonetheless, in the present paper we have chosen to keep the first term in (1), mainly for the sake of completeness.

III. Kinematics

Euler parameters[16] were chosen to describe the attitude of the spacecraft. The Euler parameters are defined in terms of the Euler principal unit vector $\hat{a}$ and angle Φ as follows

$$q_0 = \cos\frac{\Phi}{2}, \quad \bar{q} = [\, q_1 \quad q_2 \quad q_3 \,] = \hat{a} \sin\frac{\Phi}{2}.$$

The Euler parameter vector is given by $\mathbf{q} \triangleq [\, q_0 \quad \bar{q} \,]^{\mathsf{T}} \in \mathbb{R}^{4\times 1}$. The differential equation that governs the attitude kinematics in terms of the Euler parameter vector is given by[16,17]

$$\dot{q}_0 = -\tfrac{1}{2}\bar{q}^{\mathsf{T}}\omega, \quad \dot{\bar{q}} = \tfrac{1}{2}\begin{bmatrix} q_0 & -q_3 & q_2 \\ q_3 & q_0 & -q_1 \\ -q_2 & q_1 & q_0 \end{bmatrix}\begin{bmatrix} p \\ q \\ r \end{bmatrix} \triangleq \tfrac{1}{2} Q(\mathbf{q})\omega. \tag{3}$$

For the following developments it will be useful to introduce the additional variable $\eta_0 \triangleq 1 - q_0$. It can be easily verified that η_0 satisfies the differential equation

$$\dot{\eta}_0 = -\dot{q}_0 = \frac{1}{2}\bar{q}^\mathsf{T}\omega. \tag{4}$$

IV. Gravity Disturbance Adaptive Cancellation

The term in the right-hand-side of (1) represents the gravity torque owing to the misalignment between the mass center and the center of rotation of the spacecraft simulator platform. Although the spacecraft facility used in this work was carefully balanced prior to each experiment in order to faithfully represent a zero-g environment, nonetheless, perfect balancing is impossible. Therefore, there always exists a gravity torque that tends to deteriorate the performance. Since the total weight of the experimental platform is about 100 Kg, even a misalignment of 0.1 mm will result in a constant disturbance torque of approximately 100 mNm. This gravity torque has to be compensated by the controller in order to achieve accurate (better than 0.1 deg) three-axis attitude hold. A dynamic state-feedback stabilizing control law was therefore implemented to identify and cancel this disturbance torque.

The gravity torque acting on the spacecraft is given as

$$\vec{g}_e = mg\vec{r} \times \hat{n}_0 = -\hat{n}_0 \times mg\,\vec{r} \tag{5}$$

where $\vec{r}$ is the position vector from the center of rotation of the platform to the center of mass and $\hat{n}_0$ is the inertial unit vector along the local vertical (Z-axis of inertial frame is pointing downwards). When expressed in the body frame the gravity torque therefore takes the form $g_e = -mg[n_0^\times]\,r$.

If we rearrange Eq. (1) by moving all terms involving the gimbal rates and accelerations onto the right-hand side, one obtains

$$\begin{aligned} &J\dot{\omega} + [\omega^\times]^B I\omega + mg\,[n_0^\times]\,r = \\ &\quad -\dot{J}\omega - A_\mathrm{g} I_\mathrm{cg}\ddot{\gamma} - A_\mathrm{t} I_\mathrm{ws}[\Omega]^d\dot{\gamma} - [\omega^\times]\Big({}^G I(\gamma)\omega + A_\mathrm{g} I_\mathrm{cg}\dot{\gamma} + A_\mathrm{s} I_\mathrm{ws}\Omega\Big), \end{aligned} \tag{6}$$

where we have split the inertia term into the constant term ${}^B I$ and a time-varying term ${}^G I(\gamma)$ as follows

$${}^G I(\gamma) \triangleq A_\mathrm{s}(\gamma) I_\mathrm{cs} A_\mathrm{s}^\mathsf{T}(\gamma) + A_\mathrm{t}(\gamma) I_\mathrm{ct} A_\mathrm{t}^\mathsf{T}(\gamma) + A_\mathrm{g} I_\mathrm{cg} A_\mathrm{g}^\mathsf{T}. \tag{7}$$

In order to proceed, we introduce the following notation, where $v = [\ v_1\ v_2\ v_3\ ]^\mathsf{T}$ denotes any three-dimensional vector. Specifically, we can write

$${}^B I\, v = \Gamma_1^\mathsf{T}(v)\vartheta_1, \tag{8}$$

where,

$$\Gamma_1^\mathsf{T}(v) \triangleq \begin{bmatrix} v_1 & v_2 & v_3 & 0 & 0 & 0 \\ 0 & v_1 & 0 & v_2 & v_3 & 0 \\ 0 & 0 & v_1 & 0 & v_2 & v_3 \end{bmatrix}, \qquad \vartheta_1 \triangleq [\ I_\mathrm{x}\quad I_\mathrm{xy}\quad I_\mathrm{xz}\quad I_\mathrm{y}\quad I_\mathrm{yz}\quad I_\mathrm{z}\ ]^\mathsf{T}.$$

Furthermore, we have

$$[v^\times]\,{}^B I v = \Gamma_2^\mathsf{T}(v)\vartheta_1, \tag{9}$$

where,

$$\Gamma_2^{\mathsf{T}}(v) \triangleq \begin{bmatrix} 0 & -v_1v_3 & v_1v_2 & -v_2v_3 & v_2^2 - v_3^2 & v_2v_3 \\ v_1v_3 & v_2v_3 & v_2^2 - v_1^2 & 0 & -v_1v_2 & -v_1v_3 \\ -v_1v_2 & v_1^2 - v_3^2 & -v_2v_3 & v_1v_2 & v_1v_3 & 0 \end{bmatrix}.$$

Finally, we let

$$mg\,[v^{\times}]\,r = \Gamma_3^{\mathsf{T}}(v)\vartheta_2 \tag{10}$$

where $\Gamma_3^{\mathsf{T}}(v) \triangleq [v^{\times}]$ and

$$\vartheta_2 \triangleq mg\,[\begin{array}{ccc} r_x & r_y & r_z \end{array}]^{\mathsf{T}}. \tag{11}$$

Next, we let u denote all the terms involving the gimbal. That is,

$$u \triangleq -\dot{J}\omega - A_{\mathrm{g}}I_{\mathrm{cg}}\ddot{\gamma} - A_{\mathrm{t}}I_{\mathrm{ws}}[\Omega]^d\dot{\gamma} - [\omega^{\times}]\Big({}^{G}I(\gamma)\omega + A_{\mathrm{g}}I_{\mathrm{cg}}\dot{\gamma} + A_{\mathrm{s}}I_{\mathrm{ws}}\Omega\Big) \tag{12}$$

Then, using (8)-(11) one obtains the following simplified form of the equation of motion

$$\dot{\omega} = -J^{-1}\Big(\Gamma_2^{\mathsf{T}}(\omega)\vartheta_1 + \Gamma_3^{\mathsf{T}}(\hat{n}_0)\vartheta_2 - u\Big). \tag{13}$$

The proof of the following Theorem can be found in Ref. 14.

Theorem 1 (Ref. 14) *Consider the following dynamic state feedback control law*

$$u = -k_1\bar{q} - k_2\omega - \Gamma^{\mathsf{T}}(\mathbf{q},\omega)\hat{\vartheta} - \tfrac{1}{2}\Big({}^{G}I(\gamma)Q(\mathbf{q})\omega + \dot{J}\bar{q} + \dot{J}\omega\Big) \tag{14}$$

with update law

$$\dot{\hat{\theta}} = K\Gamma(\mathbf{q},\omega)(\bar{q} + \omega) \tag{15}$$

where,

$$\Gamma(q,\omega) = \begin{bmatrix} \Gamma_1(\dot{\bar{q}}) - \Gamma_2(\omega) \\ -\Gamma_3(\hat{n}_0) \end{bmatrix},$$

and where $\hat{\vartheta} \triangleq \begin{bmatrix} \hat{\vartheta}_1 & \hat{\vartheta}_2 \end{bmatrix}$ *is the estimate of the unknown vector* ϑ*,* k_1*,* k_2 *are positive numbers, and* K *is positive definite matrix. Then the closed-loop system of Eqs. (3) and (12)-(15) is globally asymptotically stable about the equilibrium point* $[\begin{array}{ccc} \eta_0 & \bar{q} & \omega \end{array}] = 0$.

The control of Theorem 1 will be used to stabilize the spacecraft platform in the experiments.

V. The CMG Steering Equation

The steering equation for a cluster of N CMGs is obtained by equating the expressions (14) and (12), and then arranging terms with respect to both the gimbal rate $\dot{\gamma}$ and the gimbal acceleration $\ddot{\gamma}$ as follows

$$\begin{aligned} & k_1\bar{q} + k_2\omega + \Gamma^{\mathsf{T}}(q,\omega)\hat{\vartheta} + \tfrac{1}{2}\Big({}^{G}I(\gamma)Q(\mathbf{q})\omega + \dot{J}\bar{q} + \dot{J}\omega\Big) \\ & \quad = \dot{J}\omega + A_{\mathrm{g}}I_{\mathrm{cg}}\ddot{\gamma} + A_{\mathrm{t}}I_{\mathrm{ws}}[\Omega]^d\dot{\gamma} + [\omega^{\times}]\Big({}^{G}I(\gamma)\omega + A_{\mathrm{g}}I_{\mathrm{cg}}\dot{\gamma} + A_{\mathrm{s}}I_{\mathrm{ws}}\Omega\Big). \end{aligned} \tag{16}$$

By defining

$$\mathbf{B} \triangleq A_{\mathrm{g}}I_{\mathrm{cg}}, \tag{17a}$$

$$\mathbf{D}\dot{\gamma} \triangleq A_{\mathrm{t}}I_{\mathrm{ws}}[\Omega]^d\dot{\gamma} + [\omega^{\times}]A_{\mathrm{g}}I_{\mathrm{cg}}\dot{\gamma} + \tfrac{1}{2}\dot{J}\omega - \tfrac{1}{2}\dot{J}\bar{q}, \tag{17b}$$

$$\mathbf{L}_{\mathrm{r}} \triangleq k_1\bar{q} + k_2\omega + \Gamma^{\mathsf{T}}(\mathbf{q},\omega)\hat{\vartheta} + [\omega^{\times}]\Big({}^{G}I(\gamma)\omega + A_{\mathrm{s}}I_{\mathrm{ws}}\Omega\Big) - \tfrac{1}{2}{}^{G}I(\gamma)Q(\mathbf{q})\omega, \tag{17c}$$

the *CMG steering equation* becomes,

$$\mathbf{B}\ddot{\gamma} + \mathbf{D}\dot{\gamma} = \mathbf{L}_{\mathrm{r}}. \tag{18}$$

Note that the time derivative of the total inertia matrix J in (17b) may be obtained as follows[15]

$$\dot{J} = {}^{G}\dot{I} = A_{\mathrm{t}}[\dot{\gamma}]^{d}(I_{\mathrm{cs}} - I_{\mathrm{ct}})A_{\mathrm{s}}^{\mathsf{T}} + A_{\mathrm{s}}[\dot{\gamma}]^{d}(I_{\mathrm{cs}} - I_{\mathrm{ct}})A_{\mathrm{t}}^{\mathsf{T}}. \tag{19}$$

Thus, the $\mathbf{D}$ matrix can be written as

$$\begin{aligned}\mathbf{D} = {} & A_{\mathrm{t}} I_{\mathrm{ws}}[\Omega]^{d} + [\omega^{\times}]A_{\mathrm{g}} I_{\mathrm{cg}} \\ & + \Big[(e_{s1}e_{t1}^{\mathsf{T}} + e_{t1}e_{s1}^{\mathsf{T}})(\omega - \bar{q}) \cdots (e_{sN}e_{tN}^{\mathsf{T}} + e_{tN}e_{sN}^{\mathsf{T}})(\omega - \bar{q})\Big](I_{\mathrm{cs}} - I_{\mathrm{ct}})\end{aligned} \tag{20}$$

It turns out that the norm of the matrix $\mathbf{B} = A_{\mathrm{g}} I_{\mathrm{cg}}$ is quite small, relative to the norm of $\mathbf{D}$ in (18). Moreover, in order to take full advantage of the torque amplification property of CMGs, the gimbal commands are need to be given at the gimbal rate (as opposed to gimbal acceleration) level.[1] Therefore, we may neglect the term $\mathbf{B}\ddot{\gamma}$ and write in lieu of (18) the steering equation

$$\mathbf{D}\dot{\gamma} = \mathbf{L}_{\mathrm{r}}. \tag{21}$$

The objective of a *CMG steering law* is to solve this equation for $\dot{\gamma}$, given any value of $\mathbf{L}_{\mathrm{r}}$.

VI. Overview of CMG Steering Laws

The matrix $\mathbf{D}$ in (21) has dimension $3 \times N$. Its maximal rank is 3 and whenever it has maximal rank, equation (21) can be solved as

$$\dot{\gamma} = \mathbf{D}^{\mathsf{T}}(\mathbf{D}\mathbf{D}^{\mathsf{T}})^{-1}\mathbf{L}_{\mathrm{r}}. \tag{22}$$

This is the basic form of most steering logics, and it is known as the Moore-Penrose (MP) solution.[1] Notice that since the system (21) is underdetermined (typically $N \geq 3$) there are more than one solutions. The MP solution (22) is the one that minimizes

$$\min_{\dot{\gamma}} \|\dot{\gamma}\|^2 \quad \text{subject to} \quad \mathbf{D}\dot{\gamma} = \mathbf{L}_{\mathrm{r}}. \tag{23}$$

The CMG singular states are defined as those for which the rank of the matrix $\mathbf{D}$ is less than three in Eq. (21). At those singular states the matrix $\mathbf{D}\mathbf{D}^{\mathsf{T}}$ is not invertible and the steering law (22) fails to produce the required torque. Note that the linear system (22) has a solution if and only if the vector $\mathbf{L}_{\mathrm{r}}$ is in the range space of the matrix $\mathbf{D}$, which is always the case if $\operatorname{rank}\mathbf{D} = 3$. If, however, $\operatorname{rank}\mathbf{D} < 3$ there exist torque vector directions (those which are normal to the range space of $\mathbf{D}$) that cannot be met. In other words, no set of gimbal commands $\dot{\gamma}$ can produce a torque along this direction. Moreover, in the vicinity of the singular states the magnitude of the gimbal rate $\dot{\gamma}$ becomes excessive, thus violating the gimbal rate constraints.

Clearly, the MP steering law fails when the rank of matrix $\mathbf{D}$ is less than three. In fact, it can be shown[11] that the solution (22) drives the gimbal angles towards singular configurations. Hence, this steering law is of limited use on a real system, unless it is augmented by some other steering logic that accommodates for the singularities. A steering logic is expected to provide singularity avoidance and/or escape, while producing the desired commanded torque as accurately as possible.

For all the reasons alluded to above, several modifications have been proposed to the baseline steering law (22) in the literature. Three of the most popular and effective ones are summarized next.

A. Singularity Robust (SR) steering logic[8, 18]

The difficulty with the baseline MP steering law in (22) is that near, or at a singularity, it is impossible to produce the desired torque using finite gimbal rates. The Singularity Robust (SR) steering law[8] is a modified version of the MP solution, and it was originally developed in Ref. 18. The main idea is to add an extra parameter to the pseudo-inverse of $\mathbf{D}$ when the system is close to the singularity, in order to keep the matrix $\mathbf{D}$ well-conditioned and invertible. The addition of this singularity avoidance parameter ensures finite gimbal rates in the vicinity of singularity. Using the SR steering logic it is possible to avoid (or transit through) singularities, albeit at the expense of some torque errors.

The SR solution is given by

$$\dot{\gamma} = \mathbf{D}^\mathsf{T}(\mathbf{D}\mathbf{D}^\mathsf{T} + \alpha \mathbf{I}_3)^{-1}\mathbf{L}_\mathrm{r} \triangleq \mathbf{D}^\dagger \mathbf{L}_\mathrm{r} \tag{24}$$

It can be shown that this expression solves the following minimization problem[11]

$$\min_{\dot{\gamma}} \{\frac{1}{2}\alpha\|\dot{\gamma}\|^2 + \frac{1}{2}\|\mathbf{D}\dot{\gamma} - \mathbf{L}_\mathrm{r}\|^2\}.$$

In (24) the parameter α is chosen to be small or zero away from the singular states and it takes a nonzero value at the singular states. A common choice is $\alpha = \alpha_0 \exp(-\det(\mathbf{D}\mathbf{D}^\mathsf{T}))$, where the constant α_0 is chosen by the designer. This steering logic is easy to implement online, but exhibits *gimbal lock*[8] in cases when the requested torque direction is parallel to the singular direction, that is, when $\mathbf{D}^\mathsf{T}\,\mathbf{L}_r = 0$. In these cases the commanded gimbal rate is zero and the gimbal is locked at the same position.

B. Singular Direction Avoidance (SDA) steering logic[9]

The idea behind the SR steering logic was to add some (small) avoidance parameter to the MP solution, so that the calculated gimbal rates are finite. In Ref. 9 the authors have proposed a different approach to deal with the singularity problem. Starting from the observation that the singularity of the matrix is determined by its smallest singular value, they have proposed to modify only this value close to singularity, as opposed to all three singular values as in (24). This approach has the benefit of ensuring a smaller torque error than the SR method.

The SDA method starts with the singular value decomposition[19] of the matrix $\mathbf{D}$

$$\mathbf{D} = USV^\mathsf{T},$$

where

$$S = \begin{bmatrix} \Sigma_{r\times r} & 0_{r\times(4-r)} \\ 0_{(3-r)\times r} & 0_{(3-r)\times(4-r)} \end{bmatrix},$$

and where $\Sigma_{r\times r} = \mathrm{diag}[\sigma_1, \cdots, \sigma_r]$, and U and V are unitary matrices of compatible dimension.

The SDA steering logic is given by

$$\dot{\gamma} = VS^\ddagger_{\mathrm{SDA}}U^\mathsf{T}\mathbf{L}_\mathrm{r} \triangleq \mathbf{D}^\ddagger\mathbf{L}_\mathrm{r}, \tag{25}$$

where,

$$S^\ddagger_{\mathrm{SDA}} = \begin{bmatrix} \frac{1}{\sigma_1} & 0 & 0 \\ 0 & \frac{1}{\sigma_2} & 0 \\ 0 & 0 & \frac{\sigma_3}{\sigma_3^2+\alpha} \\ 0 & 0 & 0 \end{bmatrix}. \tag{26}$$

The singularity avoidance parameter α is chosen such that

$$\alpha = \alpha_0 \exp(-k_\sigma \bar{\sigma}_3^2) \tag{27}$$

where, $\bar{\sigma}_3 \triangleq \sqrt{(N/3)}(\sigma_3/h_{\mathrm{ws}})$ is a nondimensional variable normalized with respect to the magnitude of the flywheel momentum h_{ws}, so that the response of the system is independent of the system size. The constants α and k_σ are selected as desired.

In Ref. 9 it was shown that adding the singularity avoidance parameter only to the smallest singular value when the singularity is approached, ensures not only finite gimbal rates, but also a smaller torque error than the SR steering logic. This result follows easily from (26).

C. Off-Diagonal Singularity Robust (o-DSR) steering logic[4]

Most recently, a new singularity avoidance steering logic was proposed by Wie in Ref. 4. Wie modifies the SR steering logic with the utilization of a weighting matrix with nonzero off-diagonal elements, instead of the use of a diagonal matrix. This steering logic is derived from the following minimization problem

$$\min_{\dot{\gamma}} \{(\mathbf{D}\dot{\gamma} - \mathbf{L}_{\mathrm{r}})^{\mathsf{T}} \mathbf{P} (\mathbf{D}\dot{\gamma} - \mathbf{L}_{\mathrm{r}}) + \dot{\gamma}^{\mathsf{T}} \mathbf{Q} \dot{\gamma}\}, \tag{28}$$

where,

$$\mathbf{P}^{-1} \equiv \mathbf{V} = \alpha \begin{bmatrix} 1 & \epsilon_3 & \epsilon_2 \\ \epsilon_3 & 1 & \epsilon_1 \\ \epsilon_2 & \epsilon_1 & 1 \end{bmatrix} > 0,$$

and

$$\mathbf{Q}^{-1} \equiv \mathbf{W} = \begin{bmatrix} W_1 & \alpha & \alpha & \alpha \\ \alpha & W_2 & \alpha & \alpha \\ \alpha & \alpha & W_3 & \alpha \\ \alpha & \alpha & \alpha & W_4 \end{bmatrix} > 0.$$

The singularity avoidance parameter α and the modulation function ϵ_i have the following form

$$\alpha = \alpha_0 \exp(-\mu \det \mathbf{D}\mathbf{D}^{\mathsf{T}}), \qquad \epsilon_i = \epsilon_0 \sin(\omega t + \phi_i).$$

The positive definite weighting matrices $\mathbf{P}$, $\mathbf{Q}$ (or, $\mathbf{V}$ and $\mathbf{W}$) in conjunction with the choice of α_0 and ϵ_0 must be carefully chosen such that $\mathbf{D}^{\mathsf{T}}\mathbf{P}\mathbf{L}_{\mathrm{r}} \neq 0$ and $\mathbf{W} \neq \mathbf{I}_4$ to obtain tolerable torque errors and gimbal rates while they are needed to escape all types of singularities and/or avoid singularity encounters.

The solution of (28) yields the steering law

$$\dot{\gamma} = \mathbf{D}^{\#}\mathbf{L}_{\mathrm{r}}, \tag{29}$$

where,

$$\begin{aligned} \mathbf{D}^{\#} &= [\mathbf{D}^{\mathsf{T}}\mathbf{P}\mathbf{D} + \mathbf{Q}]^{-1}\mathbf{D}^{\mathsf{T}}\mathbf{P} \\ &= \mathbf{Q}^{-1}\mathbf{D}^{\mathsf{T}}[\mathbf{D}\mathbf{Q}^{-1}\mathbf{D}^{\mathsf{T}} + \mathbf{P}^{-1}]^{-1} \\ &= \mathbf{W}\mathbf{D}^{\mathsf{T}}[\mathbf{D}\mathbf{W}\mathbf{D}^{\mathsf{T}} + \mathbf{V}]^{-1}. \end{aligned}$$

It was demonstrated throughout several examples in Ref. 4 that different values of W_i and/or non-zero off-diagonal elements are required to be able to escape all types of singularities including the external singularities. With the o-DSR steering logic, when the system becomes nearly singular, deliberate dither signals of increasing amplitude are effectively generated to provide an effective means for *explicitly* avoiding singularity encounters. However, it was shown that with the o-DSR steering logic, it rather approaches the singular states, and subsequently rapidly transits through the unavoidable singularities whenever needed.

VII. Description of Experimental Facility

A. Spacecraft Platform

The experimental facility used to implement the steering laws of the previous section is based on a three-axial air bearing, located at the Dynamics and Control Systems Laboratory of the School of Aerospace Engineering at the Georgia Institute of Technology, and shown in Fig. 1. The facility provides three rotational degrees of freedom as follows: ± 30 deg about x and y axes (horizontal) and 360 deg about the z axis (vertical). It was designed to support advanced research in the area of nonlinear spacecraft attitude dynamics and control. The spacecraft platform is made of a

Figure 1. The Georgia Tech three-axial spacecraft simulator.

cylindrical aluminum structure, and it is equipped with a variety of actuators and sensors: a set of cold-gas thrusters, four variable-speed control moment gyros (which can operate either in reaction wheel or CMG mode), a two-axis sun sensor, a three-axis magnetometer, a three-axis rate gyro, and an inertial measurement unit (IMU). An onboard computer and wireless ethernet connection with the host computer allow high-speed communication and real-time implementation of the control algorithms.

B. CMG Actuators

In the experiments presented in this paper only the CMG actuators were used to provide torques on the spacecraft. There are four CMG modules on the facility, mounted in the pyramid configuration with a skew angle of 54.7 deg. The CMG module is shown in Fig. 2. Each CMG module has two brushless DC motors. One of the motors controls the gimbal, while the other controls the wheel. A potentiometer measures the rotation angle of the gimbal axis. The gimbal rate signal is also available to the user via a separate I/O channel. The gimbal motor operates in gimbal rate mode via an internal PID servo loop torquing the gimbal according to a gimbal rate command. The gimbal is allowed to rotate within ± 100 deg and the maximum achievable gimbal rate is limited to ±25 deg/sec. The wheel motor is coupled directly (no gearbox) to a momentum wheel and it can provide torques along the wheel spin axis (when used in reaction wheel or VSCMG mode). In CMG mode this motor operates at a constant speed (maximum 4000 rpm). The wheel speed is controlled by an internal PID servo loop according to a specified angular momentum magnitude. Each CMG generates a maximum output torque of 768 mNm along the CMG output axis, which is orthogonal to both the gimbal and spin axes, with a maximum sustained angular momentum of 1.759 Nms.

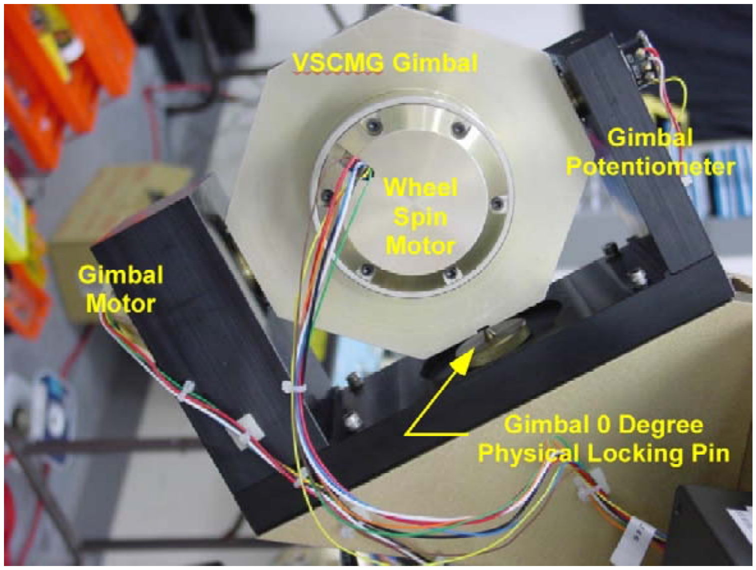

Figure 2. Main components of the CMG module.

During the experiments the magnitude of the angular momentum of each CMG $h_{\rm ws}$ was fixed to 0.6597 Nms, which corresponds to a wheel speed of 1500 rpm. The detailed physical data of each CMG are listed in Table 1.

Table 1. CMG Physical Data

Item	Value	Units
$I_{\rm ws}$	diag[0.0042, 0.0042, 0.0042, 0.0042]	kg-m^2
$I_{\rm cs}$	diag[0.0146, 0.0146, 0.0146, 0.0146]	kg-m^2
$I_{\rm cg}$	diag[0.0082, 0.0082, 0.0082, 0.0082]	kg-m^2
$I_{\rm ct}$	diag[0.0121, 0.0121, 0.0121, 0.0121]	kg-m^2
Pyramid skew angle	54.7	deg
$h_{\rm ws}$	0.6597	Nms
Gimbal angle range	±100	deg
Gimbal rate limit	±25	deg/sec

C. Communication, Computer and Electronics

An industrial embedded computer (ADLink NuPRO-775 Series) is used for data acquisition, data recording, and controller implementation via the MATLAB xPC Target Environment® with Embedded Option.[20] The main CPU is based on the Intel Pentium® III 750MHz processor with on-board memory 128MB DRAM and 128MB disk-on-chip, and it allows the user real-time data acquisition, processing, and data recording. The connection to a host computer is achieved in the xPC Target Environment via wireless Ethernet LAN connection. The wireless LAN router (DLink DI-713P) and the USB adapter (DLink DWL-120) make it possible to transfer data at speeds up to 11Mbps.

The target computer system has three data acquisition interface cards. Two analog input cards (PCI-6023E from National Instruments) are used to measure the analog voltages from the rate gyro, magnetometer, and sun sensor. Another analog output card (PCI-6703 from National Instruments) is used to control the CMGs.

A detailed description of the design and construction of this experimental spacecraft simulator facility, including the specifications for all sensors and actuators can be found in Ref. 21.

VIII. Simulation and Experimental Results

In this section we present the results from the experimental validation of the steering logics along with the dynamic state feedback stabilizing control law presented in the previous sections. The control objective in all experiments was three-axis attitude control to the zero orientation (stabilization). In order to make a reasonable and fair comparison between each steering logic, the initial conditions of attitude angles and the body angular velocity were chosen to be the same for all experiments. Specifically, the spacecraft was initially at rest at an orientation described by the Euler parameter vector $\mathbf{q}(t) = [0.96, 0.047, -0.051, 0.271]$. The objective was to reorient the spacecraft to the zero attitude using only the four CMGs as the torque generating devices. The initial gimbal angles were set to zero to allow for maximum travel before they reach their natural limits of ± 100 deg.

The gains of the feedback stabilizing control law were chosen as $k_1 = 15$, $k_2 = 40$, and $K = \mathbf{I}_9$ to achieve good performance. The singularity avoidance parameters for each steering law were carefully chosen to faithfully represent the singularity avoidance capability of each one, and to fairly compare the produced torque. The following parameters were used:

- SR steering logic

$$\alpha = 0.1 \ \exp(-\det(\mathbf{D}\mathbf{D}^{\mathsf{T}}))$$

- SDA steering logic

$$\alpha = 0.1 \ \exp(-0.5 \ k_\sigma^2)$$

- o-DSR steering logic

$$\begin{aligned} \mathbf{W} &= \operatorname{diag}[1, \ 2, \ 2, \ 3] \\ \alpha &= 0.1 \ \exp(-0.5 \ \det(\mathbf{D}\mathbf{D}^{\mathsf{T}})) \\ \epsilon_i &= \sin(t + \phi_i), \text{ where } \{\phi_1, \ \phi_2, \ \phi_3\} = \{0, \ \pi/2, \pi\} \end{aligned}$$

Figures 3-5 show the experimental results of the stabilization to the zero orientation. Figures 3(a), 4(a) and 5(a) show the Euler parameter vector history. The final values of the quaternion vector are kept to zero within 10^{-4}, which corresponds to final Euler angles of less than 0.05 deg. Figure 6 shows the final values of Euler angles for each case.

Also in Figures 3-5 the results from the numerical simulations obtained via a high fidelity Simulink® model of the whole spacecraft dynamics are shown for comparison. This model includes the details of all subsystems. Each subsystem model was constructed from the specifications of the actual components and it was identified experimentally. Particular attention was given to the parameter identification of the motors and the PID servo loops. Also, the gravity vector location was estimated and included in the model via a separate set of experiments. Details on the parameter identification and the construction of the numerical simulation model can be found in Ref. 21.

Figures 3-5 show a very similar performance for all three steering laws. The attitude and angular velocity histories are nearly identical. This implies that all three steering logics are successful in delivering the requested stabilizing torque. In addition, the agreement between the numerical simulations and the experimental results is excellent. The actual history of the quaternion and the angular velocity is remarkably identical to the one predicted by the numerical simulations. At the scale shown, the gimbal rate control inputs are also very close, but a small difference between the numerical prediction and the actual value creates a drift over time, shown in the gimbal angle histories of Figures 3(c), 4(c) and 5(c). This discrepancy can be attributed to the erroneous gravity vector estimation used in the numerical simulations. Note, in particular, that at the initial stages of the maneuver (less than 10 sec), when most of the torque produced is used for stabilization, the agreement between experiments and simulation in the gimbal angle history is very good. As the spacecraft settles to its final rest orientation, the compensation of the gravity torque dominates the total produced torque. An error in the estimation of the gravity torque thus leads to an error to the torque produced, and hence also to an error in the applied gimbal rates and resulting gimbal angles. At any rate, the dynamic state feedback control law accomplishes its stabilization task by successfully compensating the disturbance torque, regardless of the values of the gimbal angles.

As seen in Figures 3(f), 4(f) and 5(f), starting from a specific attitude the gimbal angles are initially steered towards the singular states. All three steering logics perform the transition through the singularity states at the vicinity of t=4 sec. Note that the SR and SDA steering logics failed to perform a rapid transition through the second singularity near t=35 sec. Figures 3(f), 4(f), and 5(f) show that the SR and SDA steering laws take about 35 seconds in order to transit the second singularity. On the other hand, the o-DSR steering logic transits through the second singularity faster, while staying away from the singularities for all future times.

Finally, Figures 3(e), 4(e) and 5(e) show the differences between the requested torque from the adaptive control law, $\mathbf{L}_{\mathrm{r}}$, and the actual produced torque $\mathbf{L}_{\mathrm{c}} = \mathbf{D}^{\star}\dot{\gamma}$ delivered by the CMG cluster where $\star = \dagger, \ddagger$, and $\#$, respectively. For all cases, the requested torque is very close to the torque produced by the steering logic. To better discern the differences between the three steering logics the torque errors were calculated as follows

$$L_{\mathrm{re}} = \|\mathbf{L}_{\mathrm{r}} - \mathbf{L}_{\mathrm{c}}\|_2 \tag{30}$$

Figure 7(b) shows that the torque error reaches its maximum during initialization, when the gimbals are at rest. This is due to the fact that the requested torque cannot be produced instantaneously because of the gimbal dynamics that induce a delayed response to the gimbal rate commands. Furthermore, this figure, along with Figure 7(a), also shows that the new off-Diagonal Singularity Robust steering logic has the best overall performance with good avoidance/transition through singularities and the smallest torque error.

IX. Summary and Conclusions

In this article we have experimentally compared several CMG steering laws proposed in the literature. Specifically, three singularity avoidance control laws based on the pseudo-inverse approach were tested and validated in a realistic, three-axial spacecraft simulator having a cluster of four CMGs in a pyramid configuration. An adaptive control law was implemented to stabilize the spacecraft platform, while at the same time cancelling the unknown gravity disturbance torque. The three steering logics were compared in terms of their torque error committed during singularity avoidance. All methods performed very well, with the new off-Diagonal Singularity Robust steering control law showing the best overall performance avoiding the singularities, while generating the

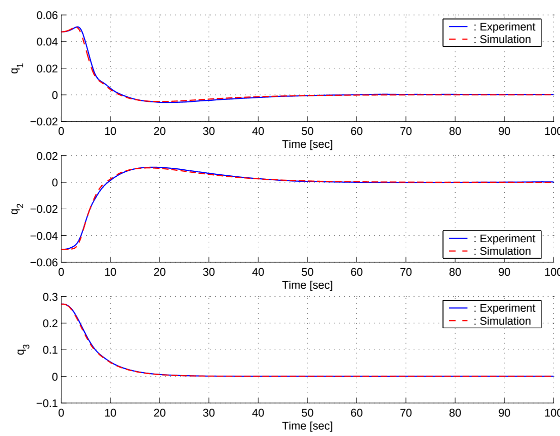

(a) Quaternion parameter

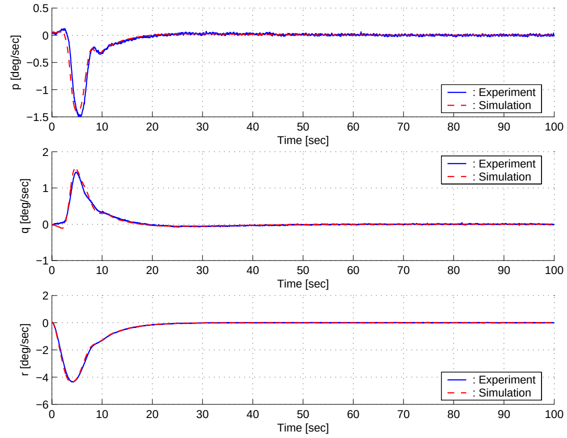

(b) Body angular rate

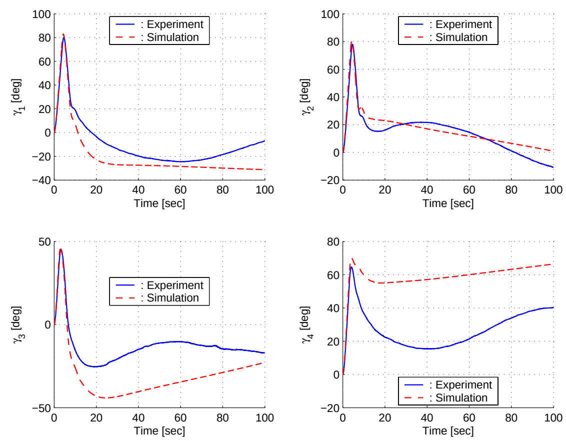

(c) Gimbal angles

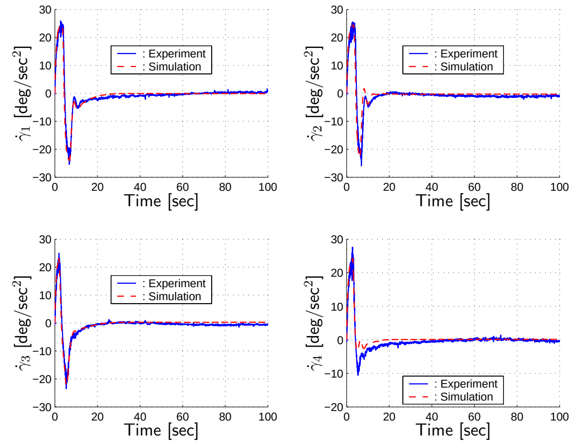

(d) Gimbal angular rates

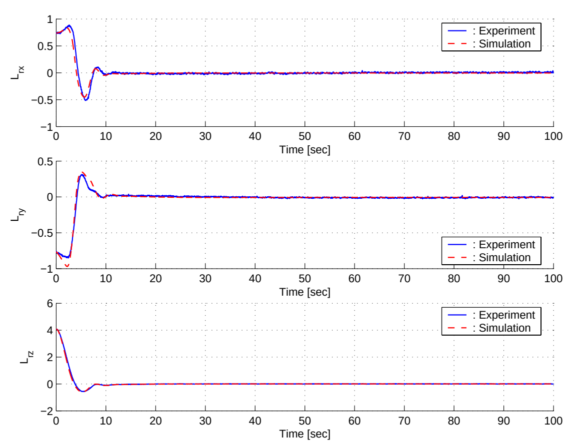

(e) Requested torque with respect to body frame

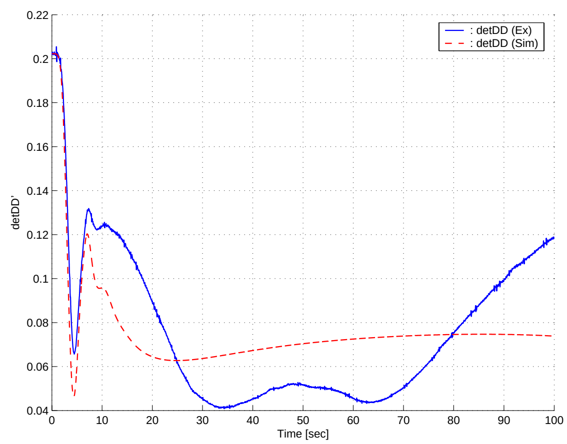

(f) Singularity measure: det$\mathbf{DD}^{\mathsf{T}}$

Figure 3. Experimental and simulated results for a reorientation maneuver utilizing the Singularity Robust (SR) steering logic.

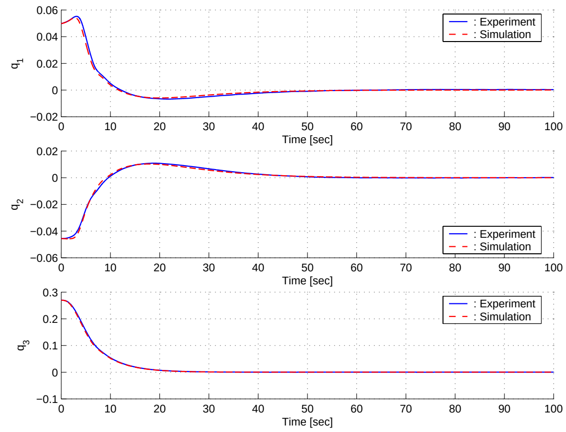

(a) Quaternion parameter

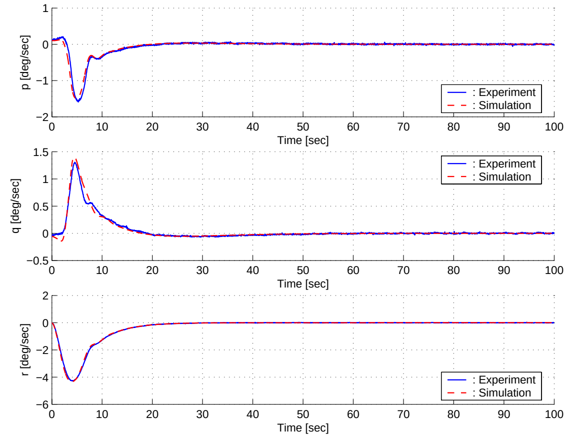

(b) Body angular rate

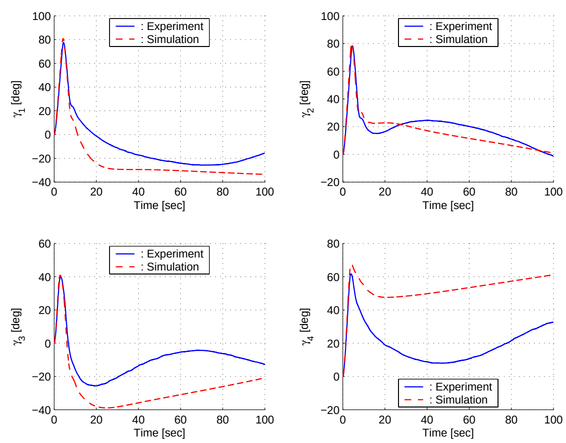

(c) Gimbal angles

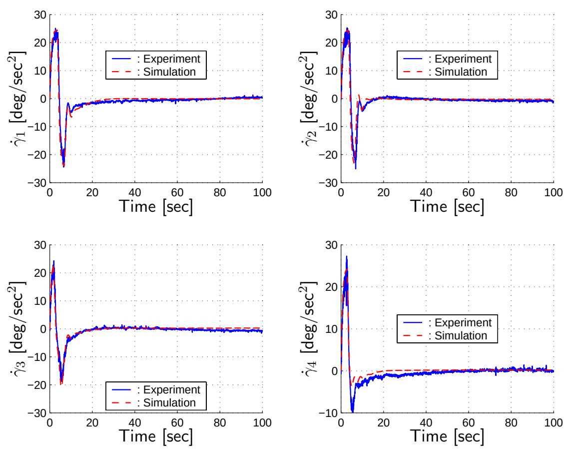

(d) Gimbal angular rates

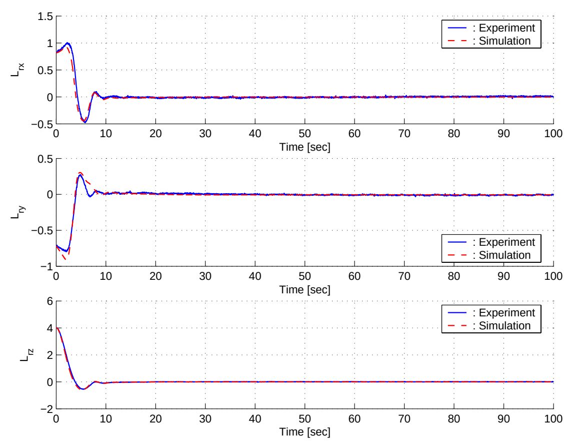

(e) Requested torque with respect to body frame

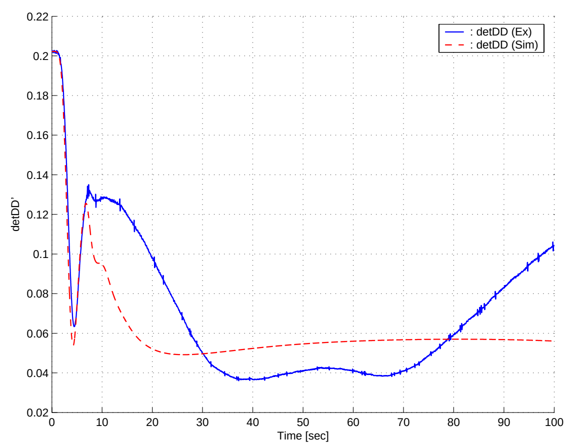

(f) Singularity measure: det$\mathbf{D}\mathbf{D}^{\mathsf{T}}$

Figure 4. Experimental and simulated results for a reorientation maneuver utilizing the Singularity Direction Avoidance (SDA) steering logic

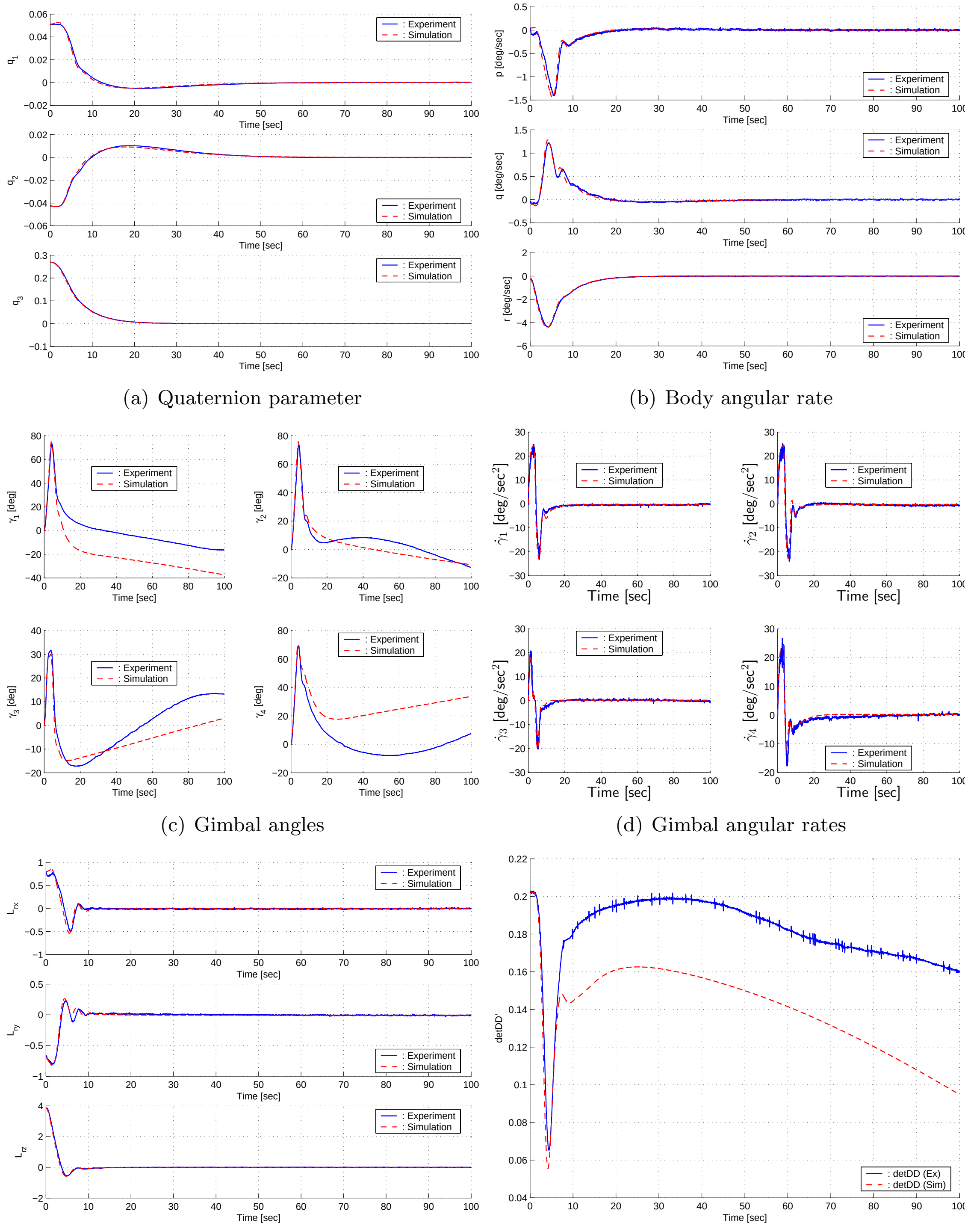

(a) Quaternion parameter

(b) Body angular rate

(c) Gimbal angles

(d) Gimbal angular rates

(e) Requested torque with respect to body frame

(f) Singularity measure: $\det \mathbf{DD}^{\mathsf{T}}$

Figure 5. Experimental and simulated results for a reorientation maneuver utilizing the off-Diagonal Singularity Robust (o-DSR) steering logic.

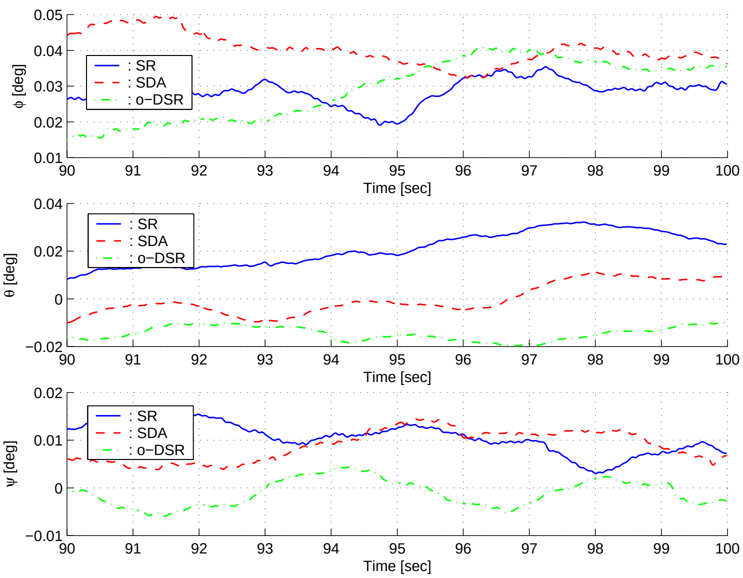

Figure 6. Final steady-state attitude in terms of Eulerian angles.

smallest torque error.

References

[1]Margulies, G. and Aubrun, J. N., "Geometric Theory of Single-Gimbal Control Moment Gyro Systems," *Journal of the Astronautical Sciences*, Vol. 26, No. 2, 1978, pp. 159–191.

[2]Bedrossian, N. S., Paradiso, J., Bergmann, E. V., and Rowell, D., "Redundant Single Gimbal Control Moment Gyroscope Singularity Analysis," *Journal of Guidance, Control, and Dynamics*, Vol. 13, No. 6, 1990, pp. 1096–1099.

[3]Kurokawa, H., "Constrained Steering Law of Pyramid-type Control Moment Gyros and Ground Test," *Journal of Guidance, Control, and Dynamics*, Vol. 20, No. 3, 1997, pp. 445–449.

[4]Wie, B., "New Singularity Escape/Avoidance Steering Logic for Control Moment Gyro Systems," *AIAA Guidance, Navigation, and Control Conference*, Austin, Texas, 2003, AIAA 2003-5659.

[5]Yoon, H. and Tsiotras, P., "Singularity Analysis and Avoidance of Variable Speed Control Moment Gyros - Part I: No Power Constraint Case," *AIAA Guidance, Navigation, and Control Conference*, Providence, Rhode Island, 2004, AIAA-2004-5207.

[6]Yoon, H. and Tsiotras, P., "Singularity Analysis and Avoidance of Variable Speed Control Moment Gyros - Part II: Power Constraint Case," *AIAA Guidance, Navigation, and Control Conference*, Providence, Rhode Island, 2004, AIAA-2004-5208.

[7]Wie, B., "Singularity Analysis and Visualization for Single-Gimbal Control Moment Gyro Systems," *Journal of Guidance, Control, and Dynamics*, Vol. 27, No. 2, 2004, pp. 271–282.

[8]Oh, H. S. and Vadali, S. R., "Feedback Control and Steering Laws for Spacecraft Using Single Gimbal Control Moment Gyros," *Journal of the Astronautical Sciences*, Vol. 39, No. 2, 1991, pp. 183–203.

[9]Ford, K. A. and Hall, C. D., "Singular Direction Avoidance Steering for Control-Moment Gyros," *Journal of Guidance, Control, and Dynamics*, Vol. 23, No. 4, 2000, pp. 648–656.

[10]Wie, B., Bailey, D., and Heiberg, C., "Singularity Robust Steering Logic for Redundant Single-Gimbal Control Moment Gyro," *Journal of Guidance, Control, and Dynamics*, Vol. 24, No. 5, 2001, pp. 865–872.

[11]Bedrossian, N. S., Paradiso, J., Bergmann, E. V., and Rowell, D., "Steering Law Design for Redundant Single-Gimbal Control Moment Gyroscopes," *Journal of Guidance, Control, and Dynamics*, Vol. 13, No. 6, 1990, pp. 1083–1089.

[12]Paradiso, J. A., "Global Steering of Single Gimballed Control Moment Gyroscopes Using a Directed Search," *Journal of Guidance, Control, and Dynamics*, Vol. 15, No. 6, 1992, pp. 1236–1244.

[13]Vadali, S. R., Oh, H. S., and Walker, S. R., "Preferred Gimbal Angles for Single Gimbal Control Moment Gyros," *Journal of Guidance, Control, and Dynamics*, Vol. 13, No. 6, 1990, pp. 1090–1095.

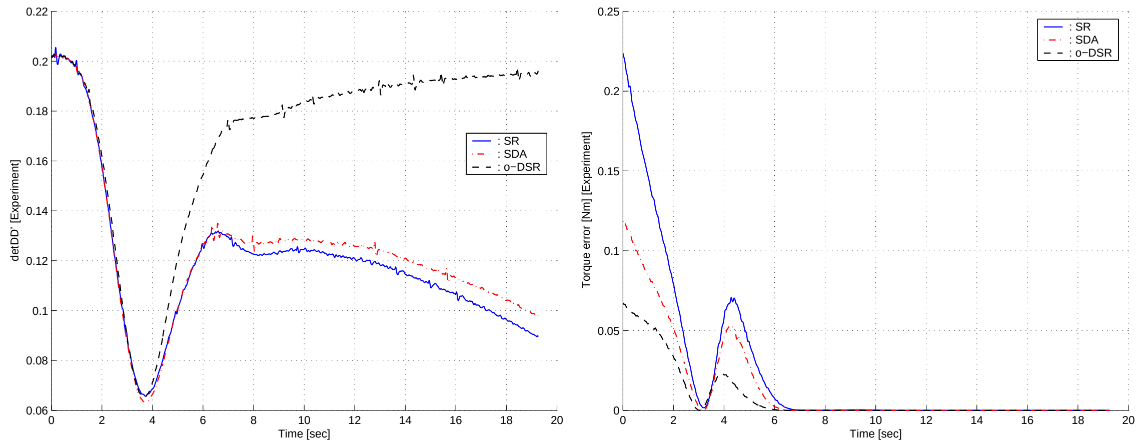

(a) Singularity measure comparison (b) Torque error comparison

Figure 7. Steering logic comparison.

[14]Di Gennaro, S., "Adaptive robust stabilization of rigid spacecraft in presence of disturbances," *Proceedings of the 34th Conference on Decision and Control*, Vol. 2, 1995, pp. 1147–1152, New Orleans, LA.

[15]Yoon, H. and Tsiotras, P., "Spacecraft Adaptive Attitude and Power Tracking with Variable Speed Control Moment Gyroscopes," *Journal of Guidance, Control and Dynamics*, Vol. 25, No. 6, 2002, pp. 1081–1090.

[16]Stevens, B. L. and Lewis, F. L., *Aircraft Control and Simulation*, John Wiley & Sons, New York, 1992.

[17]Hughes, P. C., *Spacecraft Attitude Dynamics*, John Wiley & Sons, New York, 1986.

[18]Nakamura, Y. and Hanafusa, H., "Inverse Kinematic Solutions with Singularity Robustness for Robot Manipulator Control," *Journal of Dynamic Systems, Measurement, and Control*, Vol. 108, No. 3, 1986, pp. 163–171.

[19]Horn, R. A. and Johnson, C. R., *Matrix Analysis*, Cambridge University Press, 1985.

[20]Mathworks, "xPC Target User's Guide," On-line document, http://www.mathworks.com/, 2001.

[21]Jung, D. and Tsiotras, P., "A 3-DoF Experimental Test-Bed for Integrated Attitude Dynamics and Control Research," *AIAA Guidance, Navigation, and Control Conference*, Austin, Texas, 2003, AIAA 2003-5331.